14 C and 14 C- 10 Be terrestrial age dating system for meteorites-New data for four recently fallen meteorites

Mohammad Tauseef, Ingo Leya, Jérôme Gattacceca, Beda Hofmann, Sönke Szidat, Regis Braucher

The Meteoritical Society

Meteoritics & Planetary Science 1–17 (2024)
doi: 10.1111/maps.14144

^{14}C and ^{14}C-^{10}Be terrestrial age dating system for meteorites—New data for four recently fallen meteorites

Mohammad TAUSEEF[1]*, Ingo LEYA[1], Jérôme GATTACCECA[2], Beda HOFMANN[3], Sönke SZIDAT[4], Régis BRAUCHER[2], and ASTER Team[2]

[1]Space Research and Planetary Science, Physics Institute, University of Bern, Bern, Switzerland
[2]CNRS, IRD, INRAE, CEREGE, Aix Marseille Univ, Aix-en-Provence, France
[3]Natural History Museum Bern, Bern, Switzerland
[4]Department of Chemistry, Biochemistry and Pharmaceutical Sciences, Oeschger Center for Climate Change Research, University of Bern, Bern, Switzerland

***Correspondence**
Mohammad Tauseef, Space Research and Planetary Science, Physics Institute, University of Bern, Sidlerstrasse 5, Bern 3012, Switzerland.
Email: mohammad.tauseef@unibe.ch

(Received 15 September 2023; revision accepted 22 January 2024)

Abstract–We perform a systematic and detailed study of the ^{14}C and ^{14}C-^{10}Be dating systems for meteorite terrestrial ages. Physical model calculations indicate that neither the ^{14}C production rates nor the $^{14}C/^{10}Be$ production rate ratios are constant enough to be reasonably approximated by average values. By using simple averages, one introduces a significant size-dependent bias into the database for meteorite terrestrial ages. By combining modeled ^{14}C production rates and $^{14}C/^{10}Be$ production rate ratios with $(^{22}Ne/^{21}Ne)_{cos}$ ratios and assuming ~80% ablation losses, relatively easy to use correlations of ^{14}C production rates and $^{14}C/^{10}Be$ production rate ratios as a function of $(^{22}Ne/^{21}Ne)_{cos}$ are established. The new correlations enable the determination of terrestrial ages that are more accurate than ages based solely on average values for ^{14}C and/or $^{14}C/^{10}Be$. We validate the model predictions by measuring ^{14}C activity concentrations, $^{14}C/^{10}Be$ production rate ratios, $^{21}Ne_{cos}$ concentrations, and $(^{22}Ne/^{21}Ne)_{cos}$ ratios in four recently fallen meteorites: Mt. Tazerzait, Boumdeid (2011), Bensour, and SaU 606. The experimental data confirmed the model predictions, although the available data are insufficient to be conclusive. More data from freshly fallen meteorites are needed for validating the model predictions for different chondrite sizes and chondrite types.

INTRODUCTION

Terrestrial ages of meteorites, that is, the time the meteorite spent on Earth before being found and collected, provide essential information for several highly relevant scientific questions. First, terrestrial ages are needed to better understand terrestrial weathering. For example, the conditions supporting or limiting meteorite preservations differ significantly among the different deserts. While meteorites found in the deserts of the Sultanate of Oman, North Africa, the United States, and Australia have average terrestrial ages in the range 30–50 ka (e.g., Al-Kathiri et al., 2005; Jull, 1993, 2006, 2010; Sliz et al., 2022), meteorites found in the Atacama Desert or in Antarctica can have terrestrial ages up to millions of years (e.g., Cassidy, 2003; Drouard et al., 2019; Gattacceca et al., 2011). Terrestrial ages are crucial data for comprehending and quantifying the processes involved in weathering. Second, correcting meteorite finds for pairing, that is, for determining if two meteorites belong to the same object in space that broke up during atmospheric entry, is based, among other

information, on terrestrial ages. Third, terrestrial ages are essential information to study the dynamics of small solar system bodies. In such studies, the ejection age, which is the sum of the cosmic ray exposure (CRE) age and the terrestrial age, is analyzed for a large variety of meteorites. Although in most cases, the ejection age is very similar to the CRE age, that is, the terrestrial age is short compared to the CRE age, there are meteorite classes with typically low CRE ages (lunar meteorites, carbonaceous chondrites) for which knowledge of the terrestrial age is crucial. Closely connected, studies of the meteorite influx to the Earth are all based on terrestrial ages. Relevant questions thereby are: Was the meteorite influx in a given area constant and/or was the composition of the meteorite flux variable over time? For example, studies based on sediment dispersed meteorites demonstrate that before the Paleozoic (550–250 Ma ago), the flux of LL-chondrites relative to other chondrite groups was larger than today. Data also indicate that in the Ordovician, that is, before 466 Ma, primitive achondrites had a similar or higher abundance than ordinary chondrites (e.g., Heck et al., 2017; Schmitz et al., 2017; Schmitz, Farley, et al., 2019; Schmitz, Fesit, et al., 2019). In addition, a recent study indicates that there might have been a change in the composition of the meteorite flux with a higher (compared to recent falls) abundance of H-chondrites between 1 and 0.5 million years ago (Drouard et al., 2019).

For stony meteorites, terrestrial ages are often determined using the ^{14}C and/or ^{14}C-^{10}Be dating systems (see below). Carbon-14 and ^{14}C-^{10}Be terrestrial age dating has also been applied to mesosiderites (Jull et al., 2009) and iron meteorites (Schnitzer et al., 2012). However, despite the immense potential of this dating system and the importance of the data, there are currently only three laboratories worldwide performing such studies—the University of Arizona, United States (e.g., Jull et al., 2013); the Nagoya University, Japan (Minami et al., 2006); and our group at the University of Bern (Mészáros et al., 2018; Sliz et al., 2019, 2022).

Due to analytical challenges, the ^{14}C terrestrial ages are very often not as precise and reliable as one would like them to be considering the importance of the data. For example, for calculating ^{14}C terrestrial ages, the ^{14}C saturation activity concentration at the time of fall must be known. The saturation activity concentration for a radionuclide is the saturation activity at the time of fall, that is, before any radioactive decay on Earth. It is equal to the production rate, that is, the rate of a nuclide produced per unit of mass and time during irradiation in space. In the following, we use the terms saturation activity and production rate as synonyms. For practical applications, constant (average) ^{14}C saturation activities of 46, 51.1, and 55.2 dpm kg^{-1} are used for H-, L-, and LL-chondrites, respectively (e.g., Jull et al., 1998). Generally, Jull et al. (1989, 1993, 1998) assume an uncertainty of ~15% for the production rates. The ^{14}C production rates significantly depend on shielding, which is usually not known for the studied samples. Consequently, using average values can result in a significant over- and sometimes also in a slight underestimation of the true terrestrial age. Schultz et al. (2005) was the first who applied some first-order corrections for the shielding dependence on the ^{14}C production rates by assuming a simple correlation between ^{14}C production rates and $(^{22}Ne/^{21}Ne)_{cos}$ ratios. Their approach was limited to meteorites with radii between 15 and 50 cm and they used production rates from Leya et al. (2000). However, the studied size range is rather limited and the model from Leya et al. (2000) is not very reliable for ^{14}C. This warrants a re-evaluation.

Starting the discussion with H-chondrites, Jull et al. (1989) measured for the two H-chondrite falls Richardton and Nuevo Mercurino ^{14}C activity concentrations of 34.6 ± 0.8 and 35.3 ± 0.4 dpm kg^{-1}, that is, up to 20% lower than the recommended value of 46 ± 1.0 dpm kg^{-1}. For the H6 chondrite Torino, Wieler et al. (1996) measured a ^{14}C activity concentration of 42.2 ± 2.1 dpm kg^{-1}. According to their study, Torino had a complex exposure history; the pre-atmospheric radius of the final meteorite was likely in the range of 20 cm and the second-stage exposure time was long enough that ^{14}C reached saturation (see also Herzog et al., 1991). Recently, Jull et al. (2009) measured a ^{14}C activity concentration for the H4–5 chondrite fall Carancas of 56.9 ± 1.5 dpm kg^{-1}, that is, much higher than other published values. The spread in the published data is more than 60%, which is far larger than the 15% uncertainty usually applied (e.g., Jull et al., 1998). Vogt et al. (1993) measured for the Bur Gheluai H5 chondrite fall ^{14}C activity concentrations between 37.7 and 53.1 dpm kg^{-1}, that is, the data vary by ~30%. Even larger variations were detected by Leya et al. (2001) for the H5 chondrite fall St-Robert, for which the authors determined ^{14}C activity concentrations ranging from 49 ± 12 to 75 ± 4 dpm kg^{-1}, that is, the values vary by ~50%. To summarize, the published ^{14}C saturation activities for H-chondrite falls range from 34.6 to 75 ± 4 dpm kg^{-1}, that is, they vary by more than a factor of 2. The average ^{14}C saturation activity considering all data is 51 ± 12, which agrees with the typically used value of 46 ± 1.0 dpm kg^{-1} (e.g., Jull et al., 1998) only due to the large (1σ) SD. However, the large SD leads to uncertainties of ~2 kyr (1σ) and in some cases even more than this, which can seriously limit data interpretation.

The ^{14}C saturation activities found in the literature for L-chondrites range between 44 ± 1 dpm kg^{-1} and 60.1 ± 0.9 dpm kg^{-1}, that is, they vary by more than 35% (see Minami et al., 2006 for references). In addition, the depth profile for the L/LL5 chondrite Knyahinya ranges

from 37 to 58 dpm kg^{-1} (Jull et al., 1994). The average ^{14}C saturation activity is 53.5 ± 4.4 dpm kg^{-1}, that is, reasonably close to the typically used value of 51.1 ± 1.0 dpm kg^{-1} (e.g., Jull et al., 1998), but with a much higher uncertainty. To our knowledge, there is so far no measurement of ^{14}C saturation activities for LL-chondrites.

To summarize, the data so far indicate that there is a large spread in published ^{14}C saturation activities. This finding is supported by earlier model calculations that also indicate a significant depth and size dependency of the ^{14}C production rates. For example, Wieler et al. (1996) predicted ^{14}C production rates ranging from ~12 dpm kg^{-1} for surface samples of small meteorites to ~52 dpm kg^{-1} for shielded samples in objects with pre-atmospheric radii in the range of 45 cm.

To overcome the problem of variable ^{14}C production rates, ^{14}C/^{10}Be ratios can be used instead; the ^{10}Be data serve as a proxy for the shielding dependence of the ^{14}C production rates. The ^{14}C/^{10}Be production rate ratios have been supposed to be less shielding dependent than ^{14}C production rates, making ^{14}C/^{10}Be ages more reliable than ^{14}C ages (Jull et al., 2010; Kring et al., 2001). However, the ^{14}C/^{10}Be production rate ratio and its dependence on shielding are not well constrained. In literature, one often finds an average ^{14}C/^{10}Be production rate ratio of 2.5 ± 0.1, whereas it is difficult to find the proper references and/or the underlying data. For example, for calculating the terrestrial age of the Gold Basin strewn field, Kring et al. (2001) used the ratio of 2.5 ± 0.1, giving Jull et al. (1990) as a reference. However, in their study of meteorites from western Libya, there is no mentioning of a ^{14}C/^{10}Be production rate ratio. The other reference often given, Welten et al. (2001), used a ^{14}C/^{10}Be production rate ratio of 2.65 ± 0.20 with a reference to Jull et al. (2000). In the latter study, the author has used data from a few irradiation experiments and from recently fallen meteorites (e.g., Jull et al., 1994). The actual data, however, indicate that the ^{14}C/^{10}Be production rate ratio scatters around 2.5 but with a spread of larger than 0.1. As an example, the data for Knyahinya give a ^{14}C/^{10}Be production rate ratio of 2.1 (Jull et al., 1994), that is, lower than the recommended average. In contrast, the ^{14}C/^{10}Be production rate ratio for the H chondrite Carancas is 3.3 ± 0.1 (Jull et al., 2009), that is, significantly higher than the average value. Additionally, the ^{14}C/^{10}Be production rate ratios for St-Robert (H5) vary from 2.3 to 3.7, that is, they vary by more than 60% (Leya et al., 2001). This variation is for samples from the very same meteorite, clearly contradicting the basic assumption that ^{14}C/^{10}Be production rate ratios are constant or at least relatively constant. The large spread is confirmed in a more systematic study, in which Jull et al. (2010) studied the dependence of ^{14}C/^{10}Be production rate ratios on meteoroid size and shielding. Based on model calculations, the authors found ratios between 1.2 at the surface of small meteoroids and 3.0 for deeper samples in larger meteoroids. However, the ^{14}C/^{10}Be ratio in meteoroids with pre-atmospheric sizes in the range 25–100 cm, which is a very common size for chondrites, indeed scatter around 2.5, but with a spread much larger than the very often used 0.1.

To summarize, neither the ^{14}C production rates nor the ^{14}C/^{10}Be production rate ratios are constant enough to enable accurate and reliable terrestrial age dating using only average values. In addition, the average values are not well constrained. We therefore started a systematic study to better understand and quantify ^{14}C production rates and ^{14}C/^{10}Be production rate ratios and especially their dependence on meteorite size and shielding. Doing so, we use new model calculations and we will validate the model predictions with new experimental data for recently fallen meteorites. In addition to ^{14}C and ^{10}Be activity concentrations, we also add the cosmogenic noble gases $^{21}Ne_{cos}$ and the well-known shielding indicator $(^{22}Ne/^{21}Ne)_{cos}$ to the dating system. In doing so, $(^{22}Ne/^{21}Ne)_{cos}$ is used for additional shielding corrections and $^{21}Ne_{cos}$ is used to check if ^{10}Be is in saturation. Here, we will present in some detail the model predictions and first experimental data. A more extensive database for H-, L-, and LL-chondrites will be published in a follow-up study.

NEW MODEL CALCULATIONS

The model is similar as described earlier (Leya et al., 2021). Briefly, the model is based on the particle spectra for primary and secondary particles and the cross sections for the relevant nuclear reactions. The new version of the model calculations (labeled version V03) benefits from some major improvements compared to earlier approaches. First, the particle spectra are calculated using the Geant4 toolkit (e.g., Agostinelli et al., 2003), which provides a comprehensive set of models covering all physical processes important for nuclear interactions and transport over a wide energy range, that is, from a few MeV for neutrons up to TeV for all particles. We use Geant4 to routinely and reliably calculate particle spectra for meteoroids (spherical and elliptical), planetary surfaces, and planetary atmospheres (including magnetic fields). For the calculation, we use the physics list "FTFP_INCLXX_HP." In this setup, INCL is used to treat nucleons, that is, protons and neutrons, between 1 and 20 GeV, and heavy ions, for example, ^{4}He-particles, between 0 and 3 GeV per nucleon. Importantly, the current version of INCL can reliably handle α-induced reactions and is also able to

properly treat the emission of light charged particles up to mass number $A = 8$ (Mancusi et al., 2014). Connected to this comes the second improvement; the new model generation is the first ever able to fully include primary and secondary galactic α-particles. Third, all relevant cross-sections have been adjusted according to recent changes in AMS standards and/or half-lives. Fourth, the new model gives, for the first time, uncertainties. For more information, see Leya et al. (2021).

Using the new model calculations, we calculated ^{10}Be and ^{14}C production rates for various types of meteorites and for the Apollo 15 and Apollo 17 drill cores. For the meteorites, we consider pre-atmospheric radii between 4 and 500 cm, and for the Apollo 15 and 17 drill cores, we calculated production rates down to a depth of ~450 g cm^{-2}, using a density of 1.76 and 1.83 g cm^{-3} for Apollo 15 and Apollo 17, respectively. In addition, we calculated ^{21}Ne production rates and $(^{22}Ne/^{21}Ne)_{cos}$ ratios. The modeling results are combined to test and improve the basics of the ^{14}C and ^{14}C/^{10}Be dating systems for meteorite terrestrial ages.

Before doing so, we first need to prove that the model can accurately calculate ^{14}C and ^{10}Be production rates. Figure 1 depicts modeled and experimental ^{10}Be and ^{14}C data from the L/LL5 chondrite Knyahinya (upper row) and the Apollo 15 and Apollo 17 drill cores (lower row). We start discussing the data for Knyahinya first. The ^{10}Be data are from Graf et al. (1990) and the ^{14}C data are from Jull et al. (1994). The results of the model calculations are shown by the solid black line together with the 1σ uncertainties indicated by the gray area. There are some important findings. First, the model predictions accurately describe the experimental data. The agreement is within the uncertainties. Second, the uncertainties of the model calculations increase from the surface toward the center. This is understandable considering that for both nuclides, contributions from secondary neutrons increase from the surface toward the center and such contributions are more uncertain due to less well-known neutron cross-sections. To summarize, the model is well capable of calculating ^{10}Be and ^{14}C production rates, at least in the L/LL-chondrite Knyahinya. Next, we can demonstrate that the model is able to accurately describe ^{10}Be and ^{14}C in larger objects by comparing model predictions and experimental data for Apollo drill cores (Figure 1, lower row). The ^{10}Be data for the Apollo 15 drill core are from Nishiizumi et al. (1984). The agreement for ^{10}Be is very good, all experimental data plot within the 1σ-uncertainty envelope. The comparison is more difficult for ^{14}C because the experimental database is scarce. In addition, in the only existing database (e.g., Jull et al., 1998), most of the samples are from close to the surface; hence, they are affected by solar cosmic ray (SCR) produced ^{14}C and are therefore not suitable for such a validation. This leaves only the two data at 165 and 331 g cm^{-2} for comparison. The model predictions are slightly too low by about 10%–15%, a discrepancy that has also been observed with earlier models (e.g., Jull et al., 1998). A possible explanation for too low model predictions could be a change in the solar modulation parameter, that is, a lower solar magnetic field, during the last few tens of kyrs compared to the solar activity during the last few Myrs. For example, assuming a solar modulation of $M = 550$ MV instead of $M = 650$ MV, that is, a lower solar magnetic field and consequently a higher GCR flux reaching the Moon, would bring model and experimental data into agreement. However, this is somewhat speculative and more data are needed to prove or reject this hypothesis. Anyway, these minor discrepancies are of little consequence for our study. The modeled production rates for ^{10}Be can be found at https://doi.org/10.7910/DVN/9XTHXA, the ^{14}C data can be found at https://doi.org/10.7910/DVN/6OK1HU, and the ^{22}Ne/^{21}Ne data can be found at https://doi.org/10.7910/DVN/ST5ZHC. The production rates will be constantly extended (more meteorite types) and, if needed, updated.

Production Rates for ^{14}C

Figure 2 depicts the modeled ^{14}C production rates for L-chondrites with pre-atmospheric radii between 4 and 100 cm (Figure 2a) and between 125 and 500 cm (Figure 2b). For the latter, the production rates are shown on a logarithmic scale. The jump in the depth profile at the meteorite center for the 500 cm object is due to low statistics in the Monte Carlo calculation of the flux density and has no physical meaning. For all objects with radii less or equal 80 cm, there is an increase in ^{14}C production rates with increasing shielding depth. This increase becomes larger with increasing radius; it is a factor of 1.28 for 10 cm objects and a factor of 1.55 for 80 cm objects. In addition, there is a strong dependence of the ^{14}C production rates on the pre-atmospheric radius. For example, the production rate at the center of a 10 cm object is 31.2 dpm kg^{-1}, and for a 45 cm object, it is 54.8 dpm kg^{-1}, that is, there is an increase of more than a factor of 1.75. Consequently, the model predictions clearly demonstrate that the ^{14}C production rates depend not only on the shielding depth but also on the pre-atmospheric size of the meteorite. From the data in Figure 2, it is obvious that giving one average ^{14}C production rate applicable to all sizes of L-chondrites is impossible. Depending on size and shielding, there would be either a significant over- or underestimation of the (real) ^{14}C production rate. This is made clear by the horizontal line at a ^{14}C production rate of 51.1 ± 1.0 dpm kg^{-1}, which is the average ratio very often

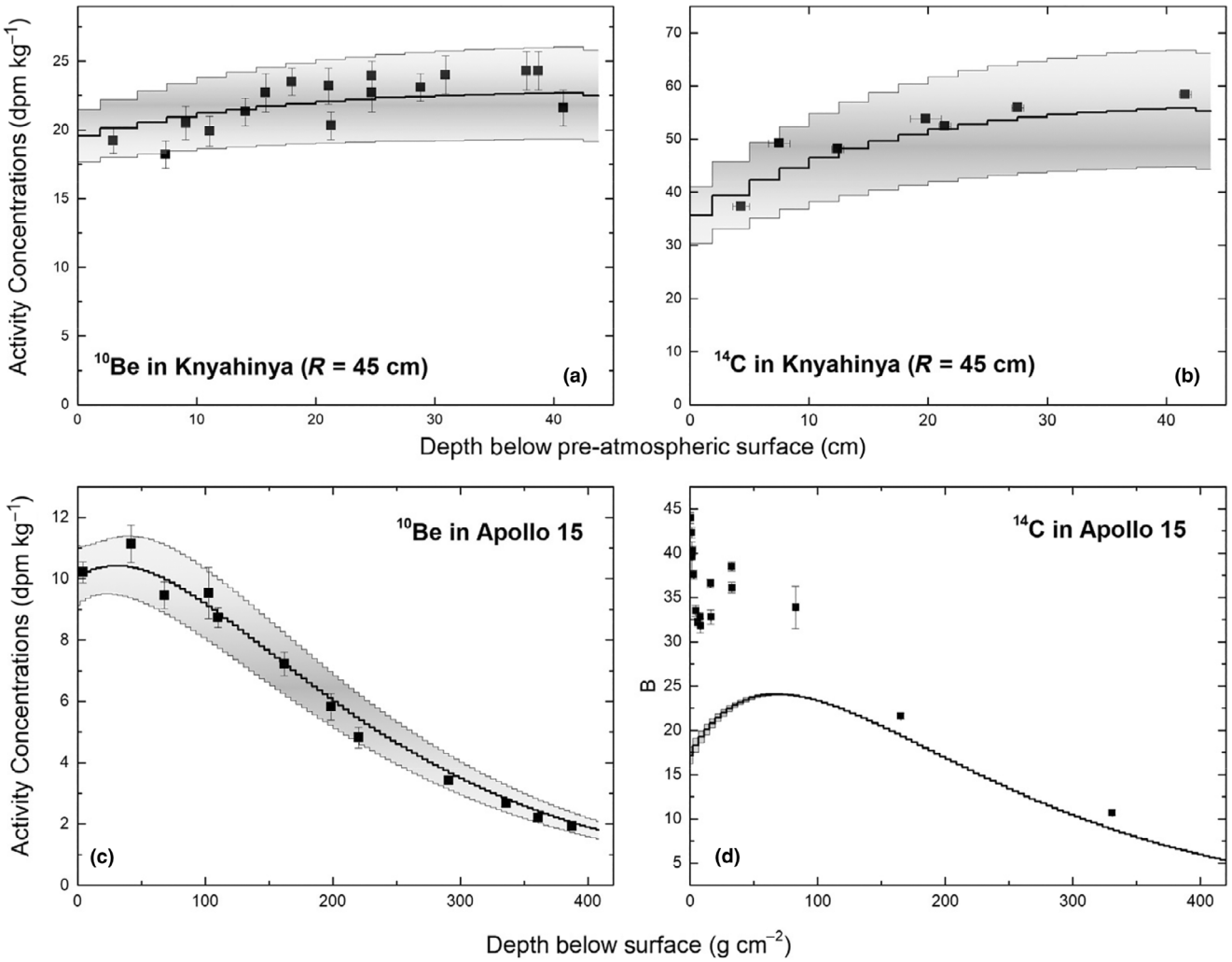

FIGURE 1. ^{10}Be and ^{14}C depth profiles for the L/LL-chondrite Knyahinya (upper row) and the Apollo 15 drill core (lower row). The experimental data are from (a) Graf et al. (1990) (^{10}Be in Knyahinya), (b) Jull et al. (1994) (^{14}C in Knyahinya), (c) Nishiizumi et al. (1984) (^{10}Be in Apollo 15), and (d) Jull et al. (1998) (^{14}C in Apollo 15). The solid black lines are the results from physical model calculations and the gray area gives 1σ uncertainties for the model predictions. The first few centimeters of the Apollo 15 drill core samples are affected by contributions from solar cosmic rays.

used for calculating ^{14}C terrestrial ages for L-chondrites (e.g., Jull et al., 1998). Considering the entire range of modeled data, which is from 21.7 to 55.2 dpm kg^{-1}, the deviation from the assumed average can reach a factor of 2.3. The consequences for the terrestrial ages are discussed below.

Using the average ^{14}C production rate of 51.1 dpm kg^{-1} is a better match for objects in the radius range 20–90 cm than it is for smaller or larger objects. Therefore, using an average production rate produces a size-dependent bias into the terrestrial age database, especially for smaller meteorites. Due to this bias, the terrestrial ages for smaller meteorites are systematically too old, which seriously compromises the interpretation of terrestrial age distribution because some samples might not necessarily be old but simply originate from smaller objects. To elaborate on this size-dependent bias, we calculated the deviation of the modeled production rate from the normally used average value as a function of meteorite size. For the calculation, we consider only the innermost 58% of each radius. Ignoring the outermost layer accounts for the typically ~80% ablation losses during atmospheric entry (in mass). Doing so, we simply assume that atmospheric entry evenly reduces the radius. The thus produced data are shown in Figure 3 as the ratio of average production rate (51.1 dpm kg^{-1}) divided by the modeled production rates as a function of pre-atmospheric radius. Since the ratios are shielding dependent, there are more data for each radius (dark gray symbols). Since the assumption of evenly distributed

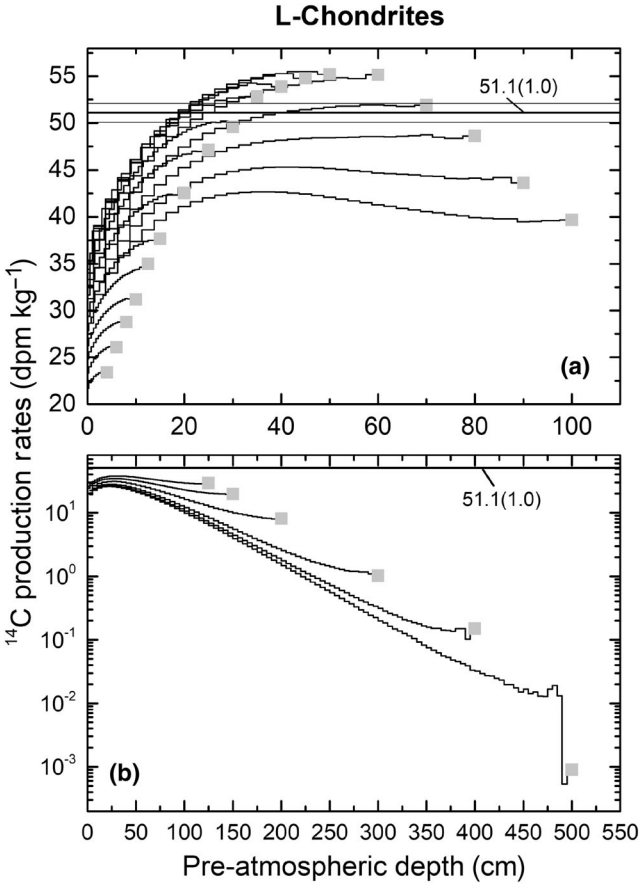

FIGURE 2. Modeled ^{14}C production rates as a function of depth below the surface for L-chondrites with pre-atmospheric radii between 4 and 100 cm (a) and with pre-atmospheric radii between 125 and 500 cm (b). Also shown is the average ^{14}C production rate of 51.1 ± 1.0 dpm kg^{-1} often used for ^{14}C terrestrial age dating of L-chondrites.

mass losses might not always be true, especially not for larger meteorites, also the data for the outermost 80% of mass, that is, 42% of the radius, are plotted (light gray symbols). The best-fit line through the data (considering ablation) is given by solid black line:

$$\text{Ratio} = 2.474 - 0.1011 \times R + 0.00242 \times R^2 - 2.503 \times 10^{-5} \times R^3 + 9.696 \times 10^{-8} \times R^4 \quad (1)$$

where R is the pre-atmospheric radius (cm) of the meteorite. The ratio between the normally assumed average production rate ratio and the modeled values can be translated into age differences. Using the equations for the radioactive decay enables calculating the ratio of terrestrial ages T_{true}, that is, the age calculated using the true production rate P_{14}(true), relative to the terrestrial age T_{av} calculated using the average production rate P_{14}(av). The obtained equation is:

$$\frac{T_{true}}{T_{av}} = 1 - \frac{\ln\left(\frac{P_{14}(true)}{P_{14}(av)}\right)}{\ln\left(\frac{A(^{14}C)}{P_{14}(av)}\right)} \quad (2)$$

where P_{14}(av) the average production rate (e.g., 51.1 dpm kg^{-1} for L-chondrites), P_{14}(true) the true production rate for ^{14}C fully considering radius and shielding dependence, and $A(^{14}C)$ the measured ^{14}C activity concentration. As an example, by assuming a measured ^{14}C activity of 25 dpm kg^{-1} and by using the average ^{14}C production rate of 51.1 dpm kg^{-1}, we calculate a terrestrial age of ~5910 years. Since the average production rate is only a good proxy for meteoroids in the size range 25–100 cm, the thus determined age is close to the "true" terrestrial age, for example, within ~10%, only for meteoroids in this size range. If the sample would originate from a small meteorite, that is, a 10 cm object, the real terrestrial age would only be ~1620 years, that is, significantly shorter. The relative differences become smaller for lower measured ^{14}C activities. For example, assuming a ^{14}C activity of 5 dpm kg^{-1} gives a nominal age (calculated using the average production rate) of ~19,200 years. If the sample originated from a small meteoroid (again assuming 10 cm), the age would be in the range of ~14,920 years, that is, significantly lower. These examples already demonstrate that using one average value for the ^{14}C production rates introduces a bias into the calculated terrestrial ages. Ages from small meteorites are overestimated, and depending on the measured ^{14}C activity concentration, this overestimation can be significant.

^{14}C/^{10}Be Production Rate Ratios

To circumvent the problem of the radius and shielding dependence of the ^{14}C production rates, the ^{14}C/^{10}Be production rate ratio is often used for calculating so-called ^{14}C-^{10}Be terrestrial ages. However, it has already been shown by Jull et al. (2004) that the ^{14}C/^{10}Be production rate ratio is not as constant as it has been assumed for reliable terrestrial age determination. Using model calculations similar to ours and studying L-chondrites with radii between 10 and 1000 cm, these authors calculated ^{14}C/^{10}Be production rates ratios ranged from ~1.2 at the surface of small meteoroids and up to ~3.0 for samples at larger shielding depths in larger meteoroids. They conclude that, for meteoroids in the size range 25–100 cm, the ^{14}C/^{10}Be ratios scatter around 2.5 but with a spread much larger than 0.1. Their results are confirmed by our new model. Figure 4a depicts the modeled ^{14}C/^{10}Be production rate ratios as a function of ^{10}Be production rates for H-chondrites with pre-atmospheric radii between 4 and 100 cm. For modeling, we again assume 80% ablation losses, that is,

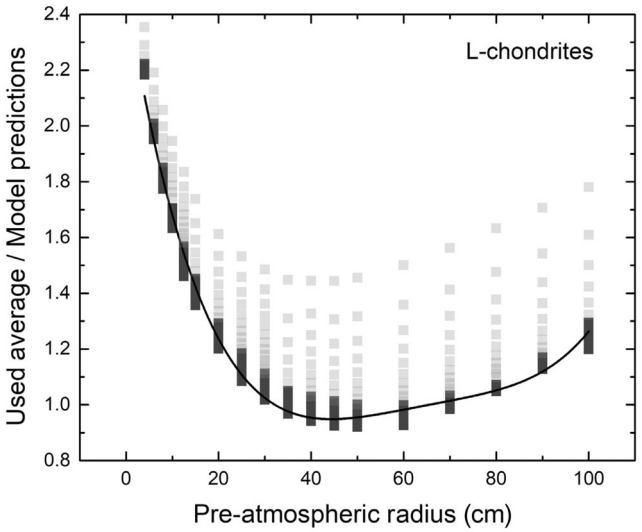

FIGURE 3. Ratio of used average ^{14}C production rate relative to the model predictions as a function of the pre-atmospheric radius of the meteoroid. For modeling, 80% ablation losses are assumed, that is, only the innermost 58% of the meteoroid is considered. The dark gray bars shown for each radius indicate the shielding dependence of the ratios for a given meteoroid radius. The light gray symbols show the data for the outermost 42% of radius, that is, for the outermost 40% of the mass. The solid black line is the best fit through the data (considering ablation).

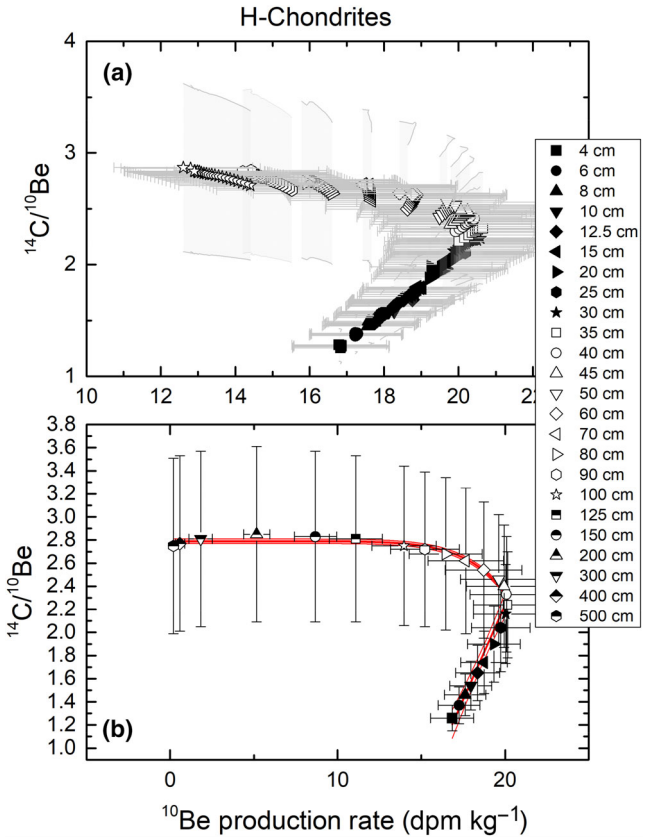

FIGURE 4. ^{14}C/^{10}Be production rate ratios as a function of ^{10}Be production rates for H-chondrites. (a) The data for meteorites with pre-atmospheric radii less or equal 100 cm. The data are for various shielding depths assuming 80% ablation losses, that is, only considering the innermost 58% of the radius. The different symbols shown for each radius indicate the data for different shielding depths. (b) The data using weighted averages and considering all meteorites with pre-atmospheric radii less or equal 500 cm. As weights, the mass for each spherical shell was used. The red line shows the best-fit line through the data.

we only consider the innermost 58% of the radius. In contrast to the earlier model, we also give uncertainties (shown by the light gray error bars). For producing the diagram shown in Figure 4b, we calculated mass weighted averages for each meteoroid, that is, we used the masses of the individual spherical shell as weights. Doing so, we produce one data point for each meteoroid (shown by the solid black symbols with error bars). Figure 4b depicts the thus calculated averages for meteoroids with pre-atmospheric radii between 4 and 500 cm. The red line is a best fit through the data.

$$\frac{^{14}\mathrm{C}}{^{10}\mathrm{Be}} = \begin{cases} a - b \times P\left(^{10}\mathrm{Be}\right)^{c} \text{ for } R \geq 35 \text{ cm} \\ f + g \times P\left(^{10}\mathrm{Be}\right) \text{ for } R < 35 \text{ cm} \end{cases} \quad (3)$$

The values for a, b, c, f, and g for H-, L-, and LL-chondrites are given in Table 1. Note that the values for the fit depend only very little on the assumption of 80% ablation losses. Considering all data and not calculating weighted averages would give correlations less than 10% different from the ones shown in Figure 4b. For pre-atmospheric radii larger than 40 cm, the ^{14}C/^{10}Be ratio varies only little with meteorite size and measured ^{10}Be concentrations, that is, for meteoroids in this size range, the average ^{14}C/^{10}Be production rate ratio is relatively constant at 2.53 ± 0.21, 2.56 ± 0.23, and 2.55 ± 0.23 for H-, L-, and LL-chondrites, respectively. However, the difficulty arises from the fact that there is no one-to-one relationship between ^{10}Be production rates and ^{14}C/^{10}Be ratios, that is, for some ^{10}Be data, there is more than one ^{14}C/^{10}Be ratio possible. As an example, for a ^{10}Be production rate of 17.5 dpm kg^{-1}, which is possible either in a 10 cm meteorite or in a 60 cm object, the ^{14}C/^{10}Be production rate ratios can be either 1.4 for small objects or 2.7 for larger objects (see Figure 4). To be more quantitative, assuming a measured ^{14}C/^{10}Be ratio of 1, 0.5, or 0.1 and a ^{14}C/^{10}Be production rate ratio of 2.7 (large object) gives terrestrial ages of 8.2, 13.9, and 27.2 kyr, respectively. In contrast, assuming a ^{14}C/^{10}Be production rate ratio of 1.4 (small object) gives terrestrial ages of 2.8, 8.5, and 21.8 kyr, respectively. Therefore, for small measured ^{14}C/^{10}Be ratios, the terrestrial ages can

TABLE 1. Parameters for the two fit functions describing the relationship of $^{14}C/^{10}Be$ production rate ratios as a function of ^{10}Be production rates (Equation 3).

Meteorite type	a	b	c	f	g
H-Chondrite	2.80 ± 0.01	$7.73 \times 10^{-10} \pm 2.11 \times 10^{-9}$	6.72 ± 0.91	-2.54 ± 0.23	0.229 ± 0.013
L-Chondrite	2.82 ± 0.01	$3.71 \times 10^{-10} \pm 1.08 \times 10^{-9}$	6.76 ± 0.95	-3.00 ± 1.44	0.237 ± 0.008
LL-Chondrite	2.80 ± 0.01	$3.12 \times 10^{-10} \pm 9.98 \times 10^{-11}$	7.50 ± 1.03	-2.90 ± 0.09	0.228 ± 0.005

Note: Valid for all radii from 4 to 500 cm. For determining the fit function, 80% ablation losses are assumed.

differ substantially depending on whether the sample is from a small or a large meteoroid. For the case $^{14}C/^{10}Be = 1.0$, the differences are almost a factor of 3. Consequently, simply using one average $^{14}C/^{10}Be$ production rate ratio for all meteorites produces a significant size-dependent bias in the terrestrial age database. However, this bias is considered relevant because it is driven not only by rarely occurring very large meteorites but also by commonly occurring small meteorites. Although the $^{14}C/^{10}Be$ dating system is more robust than ^{14}C dating because the $^{14}C/^{10}Be$ production rate ratio is constant over a larger range of meteorites sizes than the ^{14}C production rate, it can nevertheless produce some seriously wrong ages and should therefore not be applied without further knowledge of the meteorite size. In addition, the $^{14}C/^{10}Be$ production rate ratios shown in Figure 4 have relatively large uncertainties for large meteorites. This is due to the significant shielding dependence of the $^{14}C/^{10}Be$ ratio and limits the usefulness of $^{14}C/^{10}Be$ terrestrial age dating for very large objects.

To summarize, even though terrestrial ages for meteorites are highly relevant data for many applications and scientific questions, neither the ^{14}C production rates nor the $^{14}C/^{10}Be$ production rate ratios are well enough constrained for precise and reliable terrestrial age determinations.

Quantifying the Shielding Dependence of ^{14}C Production Rates

Figure 5 depicts ^{14}C production rates as a function of cosmogenic $(^{22}Ne/^{21}Ne)_{cos}$ for L-chondrites with pre-atmospheric radii of less than 90 cm. For producing the diagram, we again assume 80% ablation loses. The relationship between ^{14}C production rates and $(^{22}Ne/^{21}Ne)_{cos}$ is bijective, that is, for each $(^{22}Ne/^{21}Ne)_{cos}$ ratio, there is only one ^{14}C production rate. The relationship is given by:

$$P(^{14}C) = \left(b \times \left(^{22}Ne/^{21}Ne\right)_{cos} - a\right)^{-1} (\text{dpm per kg}) \quad (4)$$

The parameters for H-chondrites are $b = 0.099 \pm 0.001$ and $a = 0.084 \pm 0.001$. For L-chondrites: $b = 0.093 \pm 0.001$ and $a = 0.081 \pm 0.001$, and for LL-chondrites: $b = 0.091 \pm 0.001$ and $a = 0.079 \pm 0.001$. In addition to the model prediction (open symbols) and the best-fit line (solid black line), Figure 5 also shows experimental data for the L/LL-chondrite Knyahinya and the four meteorites studied by us; Mt. Tazerzait, Bensour, Boumdeid (2011), and SaU 606. The experimental data are discussed in detail below.

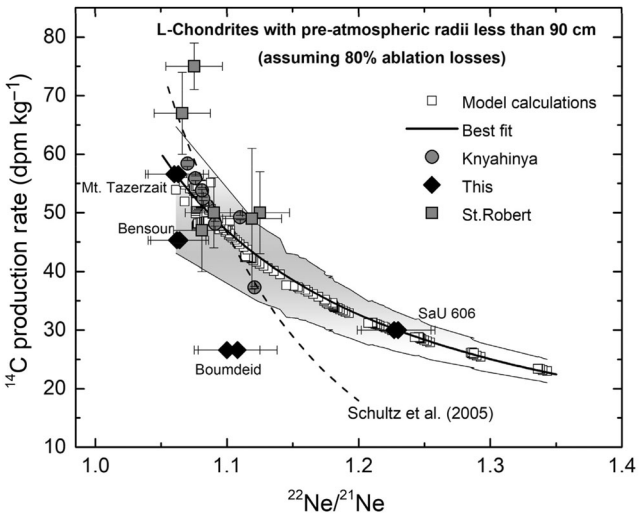

FIGURE 5. ^{14}C production rates as a function of $(^{22}Ne/^{21}Ne)_{cos}$. The model calculations for L-chondrites with radii between 4 and 90 cm are shown by the open squares. The gray area gives the 1σ standard deviation for the model calculations. The dashed line is the correlation given by Schultz et al. (2005). Also shown are experimental data for Knyahinya (Graf et al., 1990; Jull et al., 1994), St. Robert (Leya et al., 2001), and for the four meteorites studied here.

In summary, the relationship of ^{14}C production rates as a function of $(^{22}Ne/^{21}Ne)_{cos}$ enables to determine ^{14}C production rates for all shielding depths in chondrites with pre-atmospheric radii of less than 90 cm, which covers the majority of the known chondrites. Considering that $(^{22}Ne/^{21}Ne)_{cos}$ can usually be measured to within better than ~2%, the ^{14}C production rates can be determined to be within 10% for all chondrites with pre-atmospheric radii between 4 cm and less than 90 cm and for all shielding depths.

Quantifying the Shielding Dependence of ^{14}C/^{10}Be Production Rate Ratios

It is usually assumed that the ^{14}C/^{10}Be production rate ratios are less dependent on shielding than the ^{14}C production rates. We already demonstrated in Figure 4 that this is not true. Figure 6 depicts ^{14}C/^{10}Be production rate ratios as a function of the shielding indicator $(^{22}Ne/^{21}Ne)_{cos}$ ratios. The modeled data are for L-chondrites with radii between 4 and 400 cm. Again, we only consider the innermost 58% of the radius, that is, we assume 80% ablation losses. For the ^{14}C/^{10}Be ratio (open symbols), we also show the estimated uncertainties. Also shown are the experimental data for Knyahinya (Graf et al., 1990; Jull et al., 1994) and the results from our study for Mt. Tazerzait, Boumdeid (2011), Bensour, and SaU 606. The experimental data are discussed in detail below.

There is no one-to-one relationship between ^{14}C/^{10}Be production rates and $(^{22}Ne/^{21}Ne)_{cos}$ ratios, that is, the relationship is surjective. For almost all $(^{22}Ne/^{21}Ne)_{cos}$ ratios, there are two ^{14}C/^{10}Be ratios possible. For example, at a $(^{22}Ne/^{21}Ne)_{cos}$ ratio of 1.125, the ^{14}C/^{10}Be ratio can be ~1.9 for a small meteoroid (R ~20 cm) or ~2.9 for a larger object (R ~125 cm). The differences in ^{14}C/^{10}Be can be translated into terrestrial age differences. For a production rate ratio of ^{14}C/^{10}Be = 1.9 or 2.9 and a measured ^{14}C/^{10}Be of 1.0, the terrestrial ages are ~5.3 and ~8.8 ka, respectively. For a measured ratio of 0.5, the terrestrial ages are ~11.0 and ~14.5 ka. Finally, for a measured ^{14}C/^{10}Be ratio of 0.25, the terrestrial ages are ~16.7 and ~20.2 ka. Consequently, the differences in terrestrial ages can be substantial and using an average ratio introduces a significant size-dependent bias into the database.

Since the correlation ^{14}C/^{10}Be versus $(^{22}Ne/^{21}Ne)_{cos}$ is surjective, we cannot give a simple equation calculating ^{14}C/^{10}Be production rates from measured $(^{22}Ne/^{21}Ne)_{cos}$ ratios. We can, however, limit the database to produce such a one-to-one relationship. For example, if we consider only chondrites with pre-atmospheric radii less or equal 60 cm, the ambiguities disappear and the ^{14}C/^{10}Be production rate ratios can be calculated from $(^{22}Ne/^{21}Ne)_{cos}$ ratios via:

$$\frac{P(^{14}C)}{P(^{10}Be)} = a - b \times \left(^{22}Ne/^{21}Ne\right)_{cos} + c \times \left(^{22}Ne/^{21}Ne\right)^{2}_{cos} - d \times \left(^{22}Ne/^{21}Ne\right)^{3}_{cos} \quad (5)$$

The result for L-chondrites is shown by the solid black line and the 95% confidence interval is shown by the red area. The values for the parameters a, b, c, and d for H-, L-, and LL-chondrites, respectively, are given in Table 2. Note that this correlation only holds for meteorites with pre-atmospheric radii less or equal to 60 cm, which cannot easily be deduced from $(^{22}Ne/^{21}Ne)_{cos}$ ratios alone. For applying this equation, it is therefore mandatory to have an independent estimate of the pre-atmospheric size of the studied meteorite.

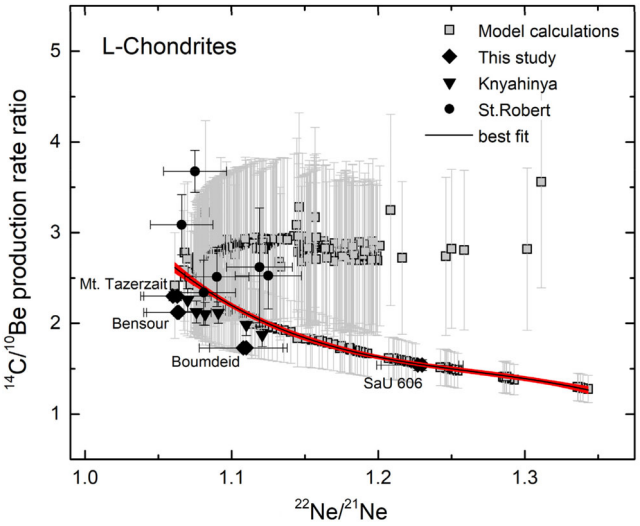

FIGURE 6. ^{14}C/^{10}Be production rate ratios as a function of $(^{22}Ne/^{21}Ne)_{cos}$. The model calculations are for L-chondrites with radii between 4 and 400 cm. The light gray error bars indicate the 1σ uncertainties of the model calculations. The red line is the best-fit line considering only meteorites with pre-atmospheric radii less or equal to 60 cm. Also shown are experimental data for Knyahinya (Graf et al., 1990; Jull et al., 1994), St. Robert (Leya et al., 2001), and the data for the four chondrites studied here. The upper branch of modeled data is for larger meteorites (pre-atmospheric radius >60 cm).

EXPERIMENTAL

Meteorite Samples

For this initiating study, four recently fallen meteorites were selected: Boumdeid (2011) (L6), Bensour (LL6), Mt. Tazerzait (L5), and Sayh al Uhaymir (SaU 606, H5). Bensour (LL6, shock stage S3) fell on February 11, 2002, at the border region between Morocco and Algeria. The total known mass of Bensour is 45 kg. Boumdeid (2011) is an L6 chondrite that fell on September 14, 2011 in the Assaba region of Mauritania. Two recent radionuclide studies (Buhl et al., 2014; Rosén et al., 2020) inferred a relatively small pre-atmospheric size for Boumdeid (2011) of radius < 20 cm, which is consistent with the small total known mass of only 3.6 kg. The L5 chondrite Mt. Tazerzait fell on August 21, 1991, near Tohua in the Republic of Niger. In total, 110 kg of

TABLE 2. Parameters for the fit function describing the relationship of $^{14}C/^{10}Be$ production rate ratios as a function of $(^{22}Ne/^{21}Ne)_{cos}$ (Equation 5).

Meteorite type	*a*	*b*	*c*	*d*
H-Chondrite	148.1 ± 12.9	345.8 ± 32.5	273.3 ± 27.2	72.4 ± 7.6
L-Chondrite	173.4 ± 13.9	403.0 ± 34.7	316.6 ± 28.7	83.3 ± 7.9
LL-Chondrite	169.0 ± 12.9	391.5 ± 32.1	306.6 ± 26.6	80.4 ± 7.3

Note: Valid for all radii from 4 to 60 cm. For determining the fit function, 80% ablation losses are assumed.

this meteorite has been recovered. Finally, SaU 606 is an H5 ordinary chondrite with shock stage S2 and a total known mass of 136.5 g. SaU 606 is not an observed fall, but an unweathered (W0) individual found in the Al-Wusta region of the Sultanate of Oman on February 12, 2017. The detectable activities of short-lived radionuclides indicate that SaU 606 fell very recently, likely in 2012 (Rosén et al., 2020). Such a short terrestrial age is negligible for ^{14}C studies; therefore, SaU 606 can be included in this study.

^{14}C Measurements and Data Reduction

Sample preparation, CO_2 extraction, and ^{14}C measurements followed the procedures recently established in our laboratory by Mészáros et al. (2018) and Sliz et al. (2019, 2022). Briefly, samples were milled and the 125–200 μm grain size fraction was selected. The samples were leached first in 6 M HCl for 30 min to dissolve carbonates and to remove any terrestrial contamination. Next, after careful drying, the samples were leached for 48 h in monoethanolamine thioglycolate (EATG) 65% to remove iron oxides and hydroxides. Leaching with 6 M HCl can also dissolve metal and troilite in addition to the weathering products and it is therefore important not to "over-leach" the samples (see Mészáros et al., 2018). However, since there is essentially no carbon in metal and troilite, the applied corrections are entirely due to mass loss during leaching, which is typically in the range of 10%–13%. Fifty milligrams of dried samples were wrapped in precleaned Al-foil and were loaded into the ^{14}C extraction line. The extracted CO_2 gas had to be spiked with ^{14}C free CO_2 to provide enough carbon (>10 μg) for the $^{14}C/^{12}C$ AMS measurements.

The measurements of the $^{14}C/^{12}C$ ratios were conducted at the MICADAS at the Laboratory for the Analysis of Radiocarbon with AMS (LARA) at the Department of Chemistry and Biochemistry, University of Bern (Szidat, 2020; Szidat et al., 2014). Briefly, the glass ampoules containing the spiked sample gas were introduced into the gas interface system (GIS) of MICADAS, cracked open, and the CO_2 was mixed with He. This mixture was then transferred to the gas ion source. A normal measurement cycle also comprises a standard reference material (Oxalic acid II; NIST, Gaithersburg, USA), and blanks, which are essentially spiked background measurements following the same procedure as for the samples. The ^{14}C results are given in fraction modern carbon ($F^{14}C$) and they account for all possible uncertainties, that is, correction for isotopic fractionation, uncertainties from blank subtraction and standard normalization, and a systematic uncertainty of 1.5‰ due to day-to-day variabilities (Szidat et al., 2014).

To determine ^{14}C activity concentrations, we followed the procedure given by Hippe et al. (2013) and Hippe and Lifton (2014) and calculated the absolute $^{14}C/^{12}C$ ratio via:

$$\left(\frac{^{14}C}{^{12}C}\right)_{S,abs} = 1.1694 \times 10^{12} \times Ab12_S \times F^{14}C_S \times \left[1 + \delta^{13}C_S\right] \times e^{(1950-y)/8223} \quad (6)$$

where $Ab12_S$ is the $^{14}C/^{12}C$ ratio of the sample determined by the observed $\delta^{13}C_S$ of the sample. $F^{14}C_S$ is the percentage of modern carbon in the sample normalized to $\delta^{13}C = -25‰_{VPDB}$ and y is the year of the measurement. Thereby, VPDB stands for Pee Dee Belemnite, a standard for the measurement of $\delta^{13}C$. The value of 1.1694×10^{-12} corresponds to the abundance of ^{14}C in modern carbon. The next step is the calculation of the number of ^{14}C atoms per gram of sample N_{14} using:

$$N_{14} = \left[\left(\frac{^{14}C}{^{12}C}\right)_{S,abs} \times N_A \times \frac{V_S}{V_A} - B\right] / M_S \text{ (atoms per g)} \quad (7)$$

where N_A as Avogadro's number (6.022×10^{-23} atoms per mole), V_S the volume of CO_2 in the sample at 20°C and 1013 mbar, and V_A the volume of 1 mol CO_2 at 20°C and 1013 mbar. B is the number of ^{14}C atoms in the blank and M_S is the mass of the sample in gram. As usual, when studying extraterrestrial samples, the final results are given as an activity concentration in disintegrations per minute per kilogram of the sample (dpm kg^{-1}) calculated via: $A_m = \lambda_{14}$ (min^{-1}) × N_{14} ×

TABLE 3. ^{14}C and ^{10}Be activity concentrations of four studied chondrites.

Sample ID	Type	Mass (mg)	$F^{14}C$[a]	N_{14} (10^6 atoms)	N_{14}[b] (10^8 atoms g^{-1})	^{14}C[c] (dpm kg^{-1})	^{10}Be (dpm kg^{-1})	^{14}C/^{10}Be
Mt. Tazerzait	L5	50.1	13.5	14.1 ± 1.5	2.81 ± 0.003	56.6 ± 0.1	24.6 ± 0.3	2.30 ± 0.05
Bensour	LL6	50.2	10.7	11.3 ± 1.3	2.25 ± 0.002	45.3 ± 0.1	21.4 ± 0.3	2.12 ± 0.04
Boumdeid	L6	50.4	6.4	6.7 ± 0.8	1.32 ± 0.001	26.6 ± 0.1	15.3 ± 0.2	1.73 ± 0.04
SaU 606	H5	50.3	6.9	7.5 ± 0.8	1.49 ± 0.002	30.0 ± 0.1	19.4 ± 0.2	1.54 ± 0.06

Note: All uncertainties are 1σ.
[a]Fraction modern carbon normalized to $\delta^{13}C$ of $-25‰_{VPDB}$ and AD 1950.
[b]N_{14} per gram sample was calculated using the sum of ^{14}C atoms from the sample and re-extraction measurements after blank correction.
[c]^{14}C activities corrected for mass loss (12.8%) from the leaching of the samples.

1000. The thus determined ^{14}C activity concentrations for the studied samples are summarized in Table 3.

^{10}Be Measurements

Sample preparation and AMS measurements of ^{10}Be were performed at the ASTER AMS facility, CEREGE, Aix-en-Provence, France. Details of the sample preparation procedure and the ^{10}Be measurements can be found in Arnold et al. (2010, 2013). In brief, ^{10}Be was extracted from 200 mg of sample material of 125–200 μm grain size. Silicate fractions were dissolved in HF, spiked with ^{9}Be carrier, and transformed into BeO powder. The BeO powder was then mixed with Niobium (Nb) powder (Aldrich, 325 mesh, 99.8%) in a 1:1.5 ratio and this mixture was pressed into the AMS cathodes. The standard reference material NIST SRM4325 with a ^{10}Be/^{9}Be ratio of $(2.79 \pm 0.03) \times 10^{-11}$ (Nishiizumi et al., 2007) and machine blanks were run before and after the samples. The measured ^{10}Be/^{9}Be ratios were corrected for procedural blanks. The AMS results include all sources of uncertainties, that is, statistical uncertainties, uncertainty of the standard, uncertainty of the mean of the standard measurements (instrumental), and a systematic uncertainty of ~0.5% (Arnold et al., 2010). Finally, the ^{10}Be data are converted to activity concentrations in dpm kg^{-1}.

Noble Gas Measurement

The measurements of the isotopic He, Ne, and Ar concentrations were following our standard procedures for stony meteorites (e.g., Leya et al., 2013). Briefly, about 20 mg samples were wrapped in Al foil and were loaded into the extraction and cleaning line. After loading, samples were heated in vacuum at ~80°C for up to 48 h to remove absorbed atmospheric gases. Samples were degassed in a Mo crucible held for 20 min at 1750°C. Blanks were regularly measured before and after sample extractions. Typical blanks (in units 10^{-12} cm^{3}STP) are ~13, ~17, and ~7 for ^{3}He, ^{4}He, and ^{20}Ne, respectively. For ^{36}Ar and ^{40}Ar, typical blanks (in 10^{-10} cm^{3}STP) are ~0.5 and ~1.1, respectively. For all samples, blanks for He and Ne isotopes contribute less than 1% to the sample gas amounts; an exception is the ^{20}Ne blank for SaU 606, which contributes ~2% to the sample gas amount. The ^{36}Ar blank contributions range from ~7% for Bensour to ~40% for one SaU 606 aliquot. The ^{40}Ar blank contributes for most samples less than 1% to the measured gas amounts, an exception is one Boumdeid (2011) aliquot, for which the blank contributes ~8%. In addition to blank corrections, the noble gas data have also been corrected for interferences and instrument nonlinearities. Calibrations were regularly performed; they consist of known amounts of standard gases having atmospheric isotopic composition. The only exception is He, which is enriched in ^{3}He relative to ^{4}He relative to terrestrial atmosphere. Released gases were cleaned using SAES® getters operating at various temperatures between 180 and 450°C. The He-Ne fraction was separated from the Ar fraction using activated charcoals held at the temperature of liquid nitrogen. The He-Ne fraction was measured in a (small volume) static sector field mass spectrometer built in-house. During the measurement, the gas was further cleaned and the background was further reduced from remaining impurities using an additional Ti getter (for the reduction of H_2) and an activated charcoal held at the temperature of liquid nitrogen to reduce hydrocarbons and Ar. The Ar fraction was purified using additional getters and was measured in a static noble gas tandem spectrometer, also built at the University of Bern, designed to minimize baseline variations caused by scattered ions. Gas concentrations are calculated by comparing the peak height of the sample signal to signals from the standards. The given noble gas data reckon all possible sources of uncertainties, including uncertainties from blank correction and uncertainties from standard measurements. We added a systematic uncertainty of 4% for the gas amounts and 2% for the isotope ratios.

RESULTS AND DISCUSSION

Noble Gases Cosmic Ray Exposure Ages and Meteorite Sizes

The noble gas results for He and Ne isotopes are summarized in Table 4. The cosmogenic values $(^{22}Ne/^{21}Ne)_{cos}$ and $^{21}Ne_{cos}$ were calculated using a two-component deconvolution with air and cosmogenic as endmembers. For the cosmogenic component, we assume $(^{20}Ne/^{22}Ne)_{cos} = 0.82$ (e.g., Dalcher et al., 2013). For all samples, two aliquots were measured; the $(^{22}Ne/^{21}Ne)_{cos}$ and $^{21}Ne_{cos}$ values for the two aliquots agree within the uncertainties, clearly demonstrating a good reproducibility. Using the $(^{22}Ne/^{21}Ne)_{cos}$ ratios, we calculated ^{21}Ne production rates based on the correlation given by Dalcher et al. (2013). The CRE ages range from 9.75 ± 0.70 Ma for one SaU 606 aliquot to 52.0 ± 2.9 Ma for one Mt. Tazerzait aliquot. Again, for all samples, the CRE ages determined from the two aliquots agree within the uncertainties.

The measured ^{36}Ar concentrations range from $\sim 3.7 \times 10^{-9}$ $cm^3STP\ g^{-1}$ for one SaU 606 aliquot to $\sim 3.0 \times 10^{-8}$ $cm^3STP\ g^{-1}$ for one Mt. Tazerzait sample. The $^{36}Ar/^{38}Ar$ ratios range between 0.72 and 4.36, indicating that measured argon is a mixture of cosmogenic and trapped argon; trapped is likely terrestrial contamination. Assuming $(^{36}Ar/^{38}Ar)_{cos} = 0.63$ and $(^{36}Ar/^{38}Ar)_{air} = 5.32$, the calculated cosmogenic $^{38}Ar_{cos}$ concentrations range between $\sim 1.7 \times 10^{-10}$ $cm^3STP\ g^{-1}$ for one SaU 606 aliquot and $\sim 1.9 \times 10^{-8}$ $cm^3STP\ g^{-1}$ for one Mt. Tazerzait sample. The reproducibility for $^{38}Ar_{cos}$ is fair. The $^{38}Ar_{cos}$ concentrations for the two aliquots from Bensour and Mt. Tazerzait agree within ~3% and ~13%, respectively. For SaU 606, both aliquots differ by a factor of ~5; the reason is not yet understood. Unfortunately, the argon phase for one Boumdeid (2011) aliquot was partly lost during extraction. All $^{40}Ar/^{36}Ar$ ratios are significantly higher than air, indicating a clear radiogenic ^{40}Ar signal. The CRE ages calculated using the correlation between $^{38}Ar_{cos}$ production rates and $(^{22}Ne/^{21}Ne)_{cos}$ given by Dalcher et al. (2013) range between 0.5 Ma for SaU 606 and 37.1 Ma for Mt. Tazerzait. All ^{38}Ar CRE ages (T_{38}) are lower than the ^{21}Ne CRE ages (T_{21}). Cole et al. (2007) found that for reasons not understood, the ^{38}Ar CRE age for Bensour is significantly lower than the ^{21}Ne CRE age. The argon isotope concentrations are summarized in Table 5.

Bensour has been analyzed for noble gases before (Cole et al., 2007) and there are some differences. The CRE ages are in good agreement, 17.8 ± 1.0 Ma and 16.0 ± 0.9 Ma measured by us and 19.3 Ma (no uncertainty is given) measured by Cole et al. (2007). The latter authors give a $(^{22}Ne/^{21}Ne)_{cos}$ ratio for Bensour of 1.123, while we measure for both aliquots much lower ratios of 1.063 ± 0.023 and 1.064 ± 0.022. There is also a discrepancy for helium. The ^3He concentrations measured by us are (all in 10^{-8} $cm^3STP\ g^{-1}$) 30.6 and 26.8, whereas Cole et al. (2007) measured a lower ^3He concentration of ~21. Unlike ^3He, our measured ^4He concentration of 1570 and 1343 (10^{-8} $cm^3STP\ g^{-1}$) is in good agreement with 1518 (10^{-8} $cm^3STP\ g^{-1}$) measured by Cole et al. (2007), clearly indicating a significant radiogenic ^4He contribution. The measured ^{38}Ar concentrations of 0.39×10^{-8} $cm^3STP\ g^{-1}$ and 0.41×10^{-8} $cm^3STP\ g^{-1}$ are surprisingly low and are not in agreement with the value of 0.73×10^{-8} $cm^3STP\ g^{-1}$ given by Cole et al. (2007).

The relatively high $(^{22}Ne/^{21}Ne)_{cos}$ ratio for SaU 606 of 1.230 ± 0.028 and 1.227 ± 0.028 suggests a small pre-atmospheric size. This finding is consistent with the conclusion by Rosén et al. (2020). Based on short-lived radionuclide data, the authors suggest a mean shielding depth for the studied sample of just a few centimeters. The argon concentrations for both aliquots are low, rendering the data unreliable.

Mt. Tazerzait has been analyzed for noble gases before by Scherer and Schultz (2001). Our results are in good agreement with their data. Both studies determine a long exposure age, for example, $T_{21} = 57.6$ Ma by Scherer and Schultz (2001) (no uncertainties are given in this study) and T_{21} of 46.5 ± 2.6 and 52.0 ± 2.9 Ma by us. The only difference is in the $(^{22}Ne/^{21}Ne)_{cos}$ ratio, which is 1.060 ± 0.022 and 1.063 ± 0.023 in our study, indicating large shielding, and 1.089 in the study by Scherer and Schultz (2001). The conclusion, however, is the same; Mt. Tazerzait comes from a shielded position and was thus part of a much larger object in space.

The measured $(^{22}Ne/^{21}Ne)_{cos}$ ratios for Boumdeid (2011) are 1.110 ± 0.025 and 1.108 ± 0.030, indicating an average-sized meteorite with a pre-atmospheric radius of around 20–40 cm. This finding agrees with a size of 10–20 cm previously reported by Buhl et al. (2014). Their estimate is based on measured ^{60}Co, ^{54}Mn, and ^{22}Na activity concentrations. The T_{21} CRE ages for Boumdeid (2011) of 25.2 ± 1.5 Ma and 23.9 ± 1.6 Ma place this meteorite well in the CRE age peak for L-chondrites.

To summarize, the CRE ages for all four studied samples are long enough that ^{10}Be has reached saturation. Therefore, all four samples can be used to validate the $^{14}C/^{10}Be$ terrestrial age dating system.

^{14}C Activities and $^{14}C/^{10}Be$ Ratios

The measured ^{14}C activity concentrations and the $^{14}C/^{10}Be$ production rate ratios are given in Table 3. The ^{14}C production rates range from 26.6 ± 0.1 dpm kg^{-1} for Boumdeid (2011) to 56.6 ± 0.1 dpm kg^{-1} for Mt. Tazerzait, that is, they vary by more than a factor of 2. The high ^{14}C activity concentration for the L5 chondrite

TABLE 4. He and Ne isotopic concentrations, cosmogenic ^{21}Ne and $(^{22}Ne/^{21}Ne)_{cos}$, and CRE ages for Bensour, SaU 606, Mt. Tazerzait, and Boumdeid.

		Concentrations in 10^{-8} cm^{3}STP g^{-1}							
Meteorite	Mass (mg)	^{3}He	^{4}He	^{20}Ne	$^{20}Ne/^{22}Ne$	$^{21}Ne/^{22}Ne$	$(^{22}Ne/^{21}Ne)_{cos}$	$^{21}Ne_{cos}$	T_{21} (Ma)
Bensour (1)	50.33	30.6 ± 1.6	1570 ± 78	7.33 ± 0.39	0.862 ± 0.019	0.938 ± 0.020	1.063 ± 0.023	8.16 ± 0.44	17.8 ± 1.0
Bensour (2)	50.89	26.8 ± 1.4	1343 ± 67	6.55 ± 0.35	0.855 ± 0.020	0.936 ± 0.020	1.064 ± 0.022	7.32 ± 0.41	16.0 ± 0.9
SaU 606 (1)	20.30	11.6 ± 0.6	1548 ± 77	1.73 ± 0.11	0.844 ± 0.026	0.811 ± 0.018	1.230 ± 0.028	1.67 ± 0.12	9.75 ± 0.70
SaU 606 (2)	20.16	13.1 ± 0.7	1599 ± 81	1.95 ± 0.15	0.886 ± 0.058	0.809 ± 0.018	1.227 ± 0.028	1.79 ± 0.18	10.29 ± 1.03
Mt. Tazerzait (1)	20.74	98.3 ± 5.2	2953 ± 148	19.36 ± 1.04	0.860 ± 0.019	0.939 ± 0.020	1.060 ± 0.022	21.7 ± 1.2	46.5 ± 2.6
Mt. Tazerzait (2)	20.29	108.0 ± 5.7	3075 ± 157	21.40 ± 1.15	0.861 ± 0.021	0.937 ± 0.020	1.063 ± 0.023	23.9 ± 1.3	52.0 ± 2.9
Boumdeid (1)	21.33	47.0 ± 2.5	1635 ± 83	8.10 ± 0.49	0.854 ± 0.020	0.898 ± 0.020	1.110 ± 0.025	9.00 ± 0.52	25.2 ± 1.5
Boumdeid (2)	21.13	45.1 ± 2.9	1595 ± 96	8.10 ± 0.49	0.855 ± 0.020	0.899 ± 0.025	1.108 ± 0.030	8.62 ± 0.56	23.9 ± 1.6

TABLE 5. Ar isotopic concentrations, cosmogenic ^{38}Ar, and CRE ages for Bensour, SaU 606, Mt. Tazerzait, and Boumdeid.

Meteorite	Mass (mg)	Concentrations in 10^{-8} cm^{3}STP g^{-1}				
		^{36}Ar	^{36}Ar/^{38}Ar	^{40}Ar/^{36}Ar	^{38}Ar$_{cos}$	T_{38} (Ma)
Bensour (1)	50.33	1.65 ± 0.33	2.51 ± 0.13	2138 ± 194	0.397 ± 0.082	7.2 ± 1.5
Bensour (2)	50.89	1.77 ± 0.36	2.56 ± 0.13	2116 ± 193	0.411 ± 0.085	7.5 ± 1.5
SaU 606 (1)	20.30	0.374 ± 0.110	4.36 ± 0.35	12,606 ± 1392	0.0177 ± 0.0015	0.5 ± 0.4
SaU 606 (2)	20.16	0.517 ± 0.130	2.91 ± 0.20	9820 ± 970	0.0923 ± 0.0041	2.8 ± 1.2
Mt. Tazerzait (1)	20.74	2.71 ± 0.55	1.32 ± 0.06	2030 ± 165	1.76 ± 0.36	32.4 ± 6.6
Mt. Tazerzait (2)	20.29	3.02 ± 0.61	1.31 ± 0.06	2031 ± 158	1.98 ± 0.40	37.1 ± 7.5
Boumdeid (1)	21.33	—	—	—	—	—
Boumdeid (2)	21.13	0.572 ± 0.139	0.72 ± 0.05	9248 ± 925	0.780 ± 0.170	17.7 ± 3.9

Mt. Tazerzait is consistent with previously reported values of 57.8 ± 0.8 and 60.1 ± 0.9 dpm kg^{-1} given by Minami et al. (2006) for the same meteorite. The average production rate for L-chondrites used so far is 51.1 ± 1.0 (Jull et al., 1998), which is only ~10% lower than the value for Mt. Tazerzait but significantly higher than the production rate of 26.6 ± 0.1 dpm kg^{-1} measured by us for the L-chondrite Boumdeid (2011).

Figure 5 depicts ^{14}C production rates as a function of $(^{22}Ne/^{21}Ne)_{cos}$ for the measured data together with model calculations (see above). Although the model calculations and therefore the best-fit line are for L-chondrites, we also plot the LL-chondrite Bensour and the H-chondrite SaU 606 in the same diagram. The differences between L- and LL-chondrites are small and are therefore of no relevance for the discussion. For H-chondrites, the model predictions and the best-fit line would be ~10% lower than for L-chondrites, the basic trend, however, would remain the same. In addition, Figure 5 depicts the correlation line (dashed line) given by Schultz et al. (2005), which is based on earlier and less reliable model calculations (e.g., Leya et al., 2000). The correlation given by Schultz et al. (2005) is significantly steeper than the correlation proposed here and is a worse fit to the experimental data. The data for Knyahinya (Graf et al., 1990; Jull et al., 1994) and the data for Mt. Tazerzait, Bensour, and SaU 606 plot within the uncertainties in the area given by the model calculations. The exception is Boumdeid (2011), for which either ^{14}C is ~50% too low or the $(^{22}Ne/^{21}Ne)_{cos}$ ratio is ~10% too low for both aliquots, which, however, show a good reproducibility. Since experimental problems can be ruled out, other hypothesis like a complex exposure history might be probable. Further studies, including more radionuclide data, are needed to finally solve this problem.

To summarize, experimental data confirm the trend given by model predictions of ^{14}C production rates as a function of $(^{22}Ne/^{21}Ne)_{cos}$. However, more experimental data are needed to properly validate the model calculations, especially independently validating them for the different chondrite sizes and types.

The measured $^{14}C/^{10}Be$ ratios range from 1.54 ± 0.06 for SaU 606 to 2.30 ± 0.05 for Mt. Tazerzait, that is, the ratios span almost the entire range of data predicted by the model calculations (see above). Figure 6 shows $^{14}C/^{10}Be$ production rate ratios as a function of $(^{22}Ne/^{21}Ne)_{cos}$. The open symbols with the light gray error bars are the results of the model calculations for L-chondrites discussed above. Also shown are the experimental data for the L/LL-chondrite Knyahinya (Graf et al., 1990; Jull et al., 1994), and the results obtained for Mt. Tazerzait, Bensour, Boumdeid (2011), and SaU 606. For the latter, each aliquot is plotted separately, that is, for each meteorite, there are two $(^{22}Ne/^{21}Ne)_{cos}$ values but only one $^{14}C/^{10}Be$ ratio. Again, we plot all data in the diagram for L-chondrites; the diagrams for H- and LL-chondrites would only be slightly different. There is a good agreement between the model calculations and the experimental data (all chondrite types). The agreement is in all cases within the uncertainties. Therefore, the experimental data clearly confirm and validate the model calculations, indicating that the $^{14}C/^{10}Be$ ratio is not constant but varies significantly with shielding, that is, with the $(^{22}Ne/^{21}Ne)_{cos}$ ratio. Again, more experimental data are needed to properly validate the model predictions.

CONCLUSIONS

We performed new and systematic model calculations for ^{10}Be and ^{14}C production rates in H-, L-, and LL-chondrites. The focus of the model calculations was on the dependence of the ^{14}C production rates on shielding to better constrain terrestrial ages for meteorites. The modeled data clearly demonstrate that using average ^{14}C production rates, as it is usually done for calculating ^{14}C terrestrial ages, is not good enough for establishing a reliable and consistent terrestrial age database. For

example, using average ^{14}C production rates introduces a size-dependent bias into the database, which can be significant, that is, it overestimates terrestrial ages for small objects and underestimates for larger objects. The introduced error can be significant. To be quantitative, assuming an L-chondrite with a pre-atmospheric radius of 10 cm, the ^{14}C production rates would rather be in the range 30 dpm kg^{-1} instead of the very often used 51.1 dpm kg^{-1}. This would have profound effects on the calculated terrestrial ages. For example, instead of the correct age of 1000 years, we would calculate 5400 years; instead of 5000 years, we would calculate 9400 years; and instead of a correct age of 10,000 years, we would calculate 14,400 years, all ages are significantly too high.

To circumvent or at least reduce the effects due to shielding, the ^{14}C/^{10}Be production rate ratio is often considered to give more reliable ages than the ^{14}C dating system. However, the model calculations clearly demonstrate that also the ^{14}C/^{10}Be ratios vary with shielding and that using an average value can produce unreliable terrestrial ages.

By combining ^{14}C production rates and ^{14}C/^{10}Be production rate ratios with the shielding indicator $(^{22}Ne/^{21}Ne)_{cos}$ and by assuming 80% ablation losses, that is, by reasonably reducing the range of data, we were able to deduce easy-to-use correlations of ^{14}C production rates and ^{14}C/^{10}Be production rate ratios as a function of $(^{22}Ne/^{21}Ne)_{cos}$. The new correlations enable determining terrestrial ages based on ^{14}C or ^{14}C/^{10}Be ratios—if combined with $(^{22}Ne/^{21}Ne)_{cos}$—more accurately than ages based solely on average values for ^{14}C and/or ^{14}C/^{10}Be. However, the higher accuracy comes with a price, in addition to ^{14}C and ^{10}Be measurements, one also needs to measure the noble gases in aliquots of the samples. This, however, is not a serious limitation because, first, reliable He and Ne noble gas measurements can be performed on sample masses of ~10 mg and, second, cosmogenic ^{21}Ne concentrations are needed to demonstrate that measured ^{10}Be is in saturation and that the ^{14}C/^{10}Be dating system can be applied. Note that the thus determined correlations depend only very little on the assumption of 80% ablation losses. Considering all data, that is, also considering regions from the very surface of the pre-atmospheric meteorite, changes the correlations only within their given uncertainties.

To validate the model predictions, we measured ^{14}C activity concentrations, ^{14}C/^{14}Be production rate ratios, $^{21}Ne_{cos}$, and $(^{22}Ne/^{21}Ne)_{cos}$ in the four recently fallen meteorite: Mt. Tazerzait (L5), Boumdeid (2011) (L6), Bensour (LL6), and in SaU 606 (H5). Although the H5 chondrite SaU 606 is not a witnessed fall, short-lived radionuclide activities indicate a very short terrestrial age of only a few years, negligible for ^{14}C and ^{14}C/^{10}Be studies. The experimental data confirmed the model predictions, though the database is too scarce to be conclusive. More data from freshly fallen meteorites are needed to properly validate the model predications, especially validating them for the different chondrite sizes and shielding depths. We therefore started a follow-up study, extending the experimental database by analyzing ^{14}C, ^{10}Be, and the noble gases in a variety of H-, L-, and LL-chondrite falls.

Acknowledgments—We thank T. Laemmal and G. Salazar for helping with the MICADAS-AMS measurements. Thanks are due to J. Wenger and S. Meier for their help in Noble Gas lab. We thank the reviewers K. C. Welten and A. J. T. Jull for their helpful and constructive reviews, which have significantly improved the manuscript. This project has been funded by the Swiss National Science Foundation grant 200020_196955. Open access funding provided by Universitat Bern.

Conflict of Interest Statement—The authors declare that they have no conflict of interests that could have appeared to influence the work reported in this paper.

Data Availability Statement—The data that support the findings of this study are openly available in the Harvard dataverse, the ^{10}Be data can be found at https://doi.org/10.7910/DVN/9XTHXA, the ^{14}C data can be found at https://doi.org/10.7910/DVN/6OK1HU, and the ^{22}Ne/^{21}Ne data can be found at https://doi.org/10.7910/DVN/ST5ZHC.

Editorial Handling—Dr. A. J. Timothy Jull

REFERENCES

Agostinelli, S., Allison, J., Amako, K., Apostolakis, J., Araujo, H., Arce, P., Asai, M., et al. 2003. GEANT4—A Simulation Toolkit. *Nuclear Instruments and Methods in Physics Research A* 506: 250–313.

Al-Kathiri, A., Hofmann, B. A., Jull, A. J. T., and Gnos, E. 2005. Weathering of Meteorites from Oman: Correlation of Chemical and Mineralogical Weathering Proxies with Terrestrial Ages of the Influence of Soil Chemistry. *Meteoritics & Planetary Science* 40: 1215–39.

Arnold, M., Aumaitre, G., Bourlès, D. L., Keddadouche, K., Braucher, R., Finkel, R. C., Nottoli, E., Benedetti, L., and Merchel, S. 2013. The French Accelerator Mass Spectrometry Facility ASTER after 4 Years: Status and Recent Developments on ^{36}Cl and ^{129}I. *Nuclear Instruments and Methods in Physics Research Section B: Beam Interactions with Material and Atoms* 294: 24–29.

Arnold, M., Merchel, S., Bourlès, D. L., Braucher, R., Benedetti, L., Finkel, R. C., Aumaitre, G., Gottdang, A., and Klein, M. 2010. The French Accelerator Mass Spectrometry ASTER: Improved Performance and Developments. *Nuclear Instruments and Methods in Physics Research Section B: Beam Interactions with Material and Atoms* 268: 1954–59.

Buhl, S., Toueirjenne, C., Hofmann, B., Laubenstein, M., and Wimmer, K. 2014. The Meteorite Fall New Boumdeid, Mauritania from September 14, 2011. *Meteorites* 3: 5–18.

Cassidy, W. A. 2003. *Meteorites, Ice, and Antarctica*. New York: Cambridge University Press.

Cole, K. J., Schultz, L., Sipiera, P. P., and Welten, K. C. 2007. Kilabo and Bensour, Two LL6 Chondrite Falls from Africa with Very Similar Mineralogical Compositions but Different Cosmic-Ray Exposure Histories. *38th Lunar and Planetary Science Conference*, abstract #1338, pp. 1477.

Dalcher, N., Caffee, M. W., Nishiizumi, K., Welten, K. C., Vogel, N., Wieler, R., and Leya, I. 2013. Calibration of Cosmogenic Noble Gas Production in Ordinary Chondrites Based on ^{36}Cl-^{36}Ar Ages. Part 1: Refined Production Rates for Cosmogenic ^{21}Ne and ^{38}Ar. *Meteoritics & Planetary Science* 48: 1841–62.

Drouard, A., Gattacceca, J., Hutzler, A., Rochette, P., Braucher, R., Bourlès, D., ASTER Team, et al. 2019. The Meteorite Flux of the Past 2 m.y. Recorded in the Atacama Desert. *Geology* 47: 673–76.

Gattacceca, J., Valenzuela, M., Uehara, M., Jull, A. J. T., Giscard, M., Rochette, P., Braucher, R., et al. 2011. The Densest Meteorite Collection Area in Hot Deserts: The San Juan Meteorite Field (Atacama Desert, Chile). *Meteoritics & Planetary Science* 46: 1276–87.

Graf, T., Signer, P., Wieler, R., Herpers, U., Sarafin, R., Vogt, S., Fieni, C., et al. 1990. Cosmogenic Nuclides and Nuclear Tracks in the Chondrite Knyahinya. *Geochimica et Cosmochimica Acta* 54: 2511–30.

Heck, P. R., Schmitz, B., Bottke, W., Rout, S. S., Kita, N. T., Cronholm, A., Defouilloy, C., Dronov, A., and Terfel, F. 2017. Rare Meteorites Common in the Ordovician Period. *Nature Astronomy* 1: id 0035.

Herzog, G. F., Vogt, S., Aylmer, D., Signer, P., Graf, T., Wieler, R., Tuniz, C., et al. 1991. Multi-Stage Exposure History of the Torino, H6, Meteorite. *22nd Lunar and Planetary Science Conference*, abstract #1280: 563–64.

Hippe, K., Kober, F., Wacker, L., Fahrni, S. M., Ivy-Ochs, S., Akar, N., Schlüchter, C., and Wieler, R. 2013. An Update on In Situ Cosmogenic ^{14}C Analysis at ETH Zürich. *Nuclear Instruments and Methods in Physics Research B* 294: 81–86.

Hippe, K., and Lifton, L. 2014. Calculating Isotope Ratios and Nuclide Concentrations for in Situ Cosmogenic ^{14}C Analyses. *Radiocarbon* 56: 1167–74.

Jull, A. J. T. 2006. Terrestrial Ages of Meteorites. In *Meteorites and the Early Solar System II*, edited by D. Lauretta, and H. Y. McSween, Jr., 889–905. Tucson, AZ: The University of Arizona Press.

Jull, A. J. T., Bland, P., Klandrud, S. E., McHargue, L. R., Bevan, A. W. R., Kring, D., and Wlotzka, F. 2000. Using ^{14}C and ^{14}C-^{10}Be for Terrestrial Ages of Desert Meteorites. In *Workshop on Extraterrestrial Material from Cold and Hot Deserts*, edited by L. Schultz, I. Franchi, A. Reid, and M. Zolensky, 41–43. LPI Contribution No. 997. Houston, TX: Lunar and Planetary Institute.

Jull, A. J. T., Bland, P. A., Bevan, A. W. R., Klandrud, S. E., and McHargue, L. R. 2001. ^{14}C and ^{14}C-^{10}Be Terrestrial Ages of Meteorites from Western Australia (Abstract). *Meteoritics & Planetary Science* 36: A91.

Jull, A. J. T., Cloudt, S., and Cielaszyk, E. 1998. ^{14}C Terrestrial Ages of Meteorites from Victoria Land, Antarctica, and the Infall Rates of Meteorites. *Geological Society London, Special Publication* 150: 75–91.

Jull, A. J. T., Donahue, D. J., Cielaszyk, E., and Wlotzka, F. 1993. Carbon-14 Terrestrial Ages and Weathering of 27 Meteorites from the Southern High Plains and Adjacent Areas (USA). *Meteoritics & Planetary Science* 28: 188–195.

Jull, A. J. T., Donahue, D. J., and Linick, T. W. 1989. Carbon-14 Activities in Recently Fallen Meteorites and Antarctic Meteorites. *Geochimica et Cosmochimica Acta* 53: 2095–2100.

Jull, A. J. T., Donahue, D. J., Reedy, R. C., and Masarik, J. 1994. A Carbon-14 Depth Profile in the L5 Chondrite Knyahinya. *Meteoritics* 29: 649–738.

Jull, A. J. T., Giscard, M. D., Hutzler, A., Schnitzer, C. J., Zahn, D., Burr, G. S., McHargue, L. R., and Hill, D. 2013. Radionuclide Studies of Stony Meteorites from Hot Deserts. *Radiocarbon* 55: 1779–89.

Jull, A. J. T., Giscard, M. D., McHargue, L. R., Kim, K. J., and Reedy, R. C. 2009. Production Rates of ^{14}C and ^{10}Be in Vaca Muerta (Mesosiderite), Carancas, and some Recent Falls (Abstract). *Meteoritics & Planetary Science* 72: 5276.

Jull, A. J. T., Kim, K. J., Reedy, R. C., McHargue, L. R., and Johnson, J. A. 2004. Modeling of ^{14}C and ^{10}Be Production Rates in Meteorites and Lunar Samples. *25th Lunar and Planetary Science Conference*, abstract #1191.

Jull, A. J. T., McHargue, L. R., Bland, P. A., Greenwood, R. C., Bevan, A. W. R., et al. 2010. Terrestrial Ages of Meteorites from the Nullarbor Region, Australia, Based on ^{14}C and ^{14}C–^{10}Be Measurements. *Meteoritics & Planetary Science* 45: 1271–83.

Jull, A. J. T., Wlotzka, F., Palme, H., and Donahue, D. J. 1990. Distribution of Terrestrial Ages and Petrologic Type of Meteorites from Western Libya. *Geochimica et Cosmochimica Acta* 54: 2895–99.

Kring, D. A., Jull, A. J. T., McHargue, L. R., Bland, P. A., Hill, D. H., and Berry, F. J. 2001. Gold Basin Meteorite Strewn Field, Mojave Desert, Northwestern Arizona: Relic of a Small Late Pleistocene Impact Event. *Meteoritics & Planetary Science* 36: 1057–66.

Leya, I., Ammon, K., Cosarinsky, M., Dalcher, N., Gnos, E., Hofmann, B., and Huber, L. 2013. Light Noble Gases in 12 Meteorites from the Omani Desert, Australia, Mauritania, Canada and Sweden. *Meteoritics & Planetary Science* 48: 1401–14.

Leya, I., Hirtz, J., and David, J.-C. 2021. Galactic Cosmic Rays, Cosmic-Ray Variations, and Cosmogenic Nuclides in Meteorites. *The Astrophysical Journal* 910: 136 17 pp.

Leya, I., Lange, H.-J., Neumann, S., Wieler, R., and Michel, R. 2000. The Production of Cosmogenic Nuclides in Stony Meteoroids by Galactic Cosmic Ray Particles. *Meteoritics & Planetary Science* 35: 259–286.

Leya, I., Wieler, R., Aggrey, K., Herzog, G. F., Schnabel, C., Metzler, K., Hildebrand, A. R., et al. 2001. Exposure History of the St-Robert (H5) Fall. *Meteoritics & Planetary Science* 36: 1479–94.

Mancusi, D., Boudard, A., Cugnon, J., David, J.-C., Pekka, K., and Leray, S. 2014. Extension of the Liège Intranuclear-Cascade Model to Reactions Induced by Light Nuclei. *Physical Review C* 90: p054602.

Mészáros, M., Leya, I., Hofmann, B., and Szidat, S. 2018. Current Performance and Preliminary Results of a New ^{14}C Extraction Line for Meteorites at the University of Bern. *Radiocarbon* 60: 601–615.

Minami, M., Terui, A., Takaoka, N., and Nakamura, T. M. 2006. An Improved Extraction System to Measure Carbon-14 Terrestrial Ages of Meteorites and Paring

of the Antarctic Yamato-75097 Group Chondrites. *Meteoritics & Planetary Science* 49(4): 529–540. https://doi.org/10.1111/j.1945–5100.2006.tb00480.

Nishiizumi, K., Elmore, D., Ma, X. Z., and Arnold, J. R. 1984. ^{10}Be and ^{36}Cl Depth Profiles in an Apollo 15 Drill Core. *Earth and Planetary Science Letters* 70: 157–163.

Nishiizumi, K., Imamura, M., Caffee, M. W., Southon, J. R., Finkel, R. C., and McAninch, J. 2007. Absolute Calibration of ^{10}Be AMS Standards. *Nuclear Instruments and Methods in Physics Research Section B: Beam Interactions with Materials and Atoms* 258: 403–413.

Rosén, A. V., Hofmann, B. A., von Sievers, M., and Schumann, M. 2020. Radionuclide Activities in Recent Chondrite Falls Determined by Gamma-Ray Spectrometry: Implications for Terrestrial Age Estimates. *Meteoritics & Planetary Science* 55: 149–163.

Scherer, P., and Schultz, L. 2001. Noble Gases in Baszkówka and Mt Tazerzait. *Geological Quarterly* 45: 313–14.

Schmitz, B., Farley, K. A., Goderis, S., Heck, P. R., Bergström, S. M., Boschi, S., Claeys, P., et al. 2019. An Extraterrestrial Trigger for the Mid-Ordovician Ice Age: Dust from the Breakup of the L-Chondrite Parent Body. *Science Advances* 5: eaax4184.

Schmitz, B., Fesit, R., Meier, M. M. M., Martin, E., Heck, P. R., Lenaz, D., Topa, D., et al. 2019. The Micrometeorite Flux to Earth during the Frasnian-Famennian Transition Reconstructed in the Coumiac GSSP Section, France. *Earth and Planetary Science Letters* 522: 234–243.

Schmitz, B., Heck, P. R., Alvarez, W., Kita, N. T., Rout, S. S., Cronholm, A., Defouilloy, C., Martin, E., Smit, J., and Terfelt, F. 2017. Meteorite Flux to Earth in the Early Cretaceous as Reconstructed from Sediment-Dispersed Extraterrestrial Spinels. *Geology* 45: 807–810.

Schnitzer, C. J., Jull, A. J. T., Biddulph, D., Zahn, D., Cheng, L., Burr, G. S., and McHargue, L. 2012. New Studies of ^{14}C and ^{10}Be in Iron Meteorites (Abstract). *Meteoritics & Planetary Science* 75: 5085.

Schultz, L., Franke, L., and Bevan, A. W. R. 2005. Noble Gases in Ten Nullarbor Chondrites: Exposure Ages, Terrestrial Ages and Weathering Effects. *Meteoritics & Planetary Science* 40: 659–664.

Sliz, M. U., Espic, C., Hofmann, B. A., Leya, I., and Szidat, S. 2019. An Update on the Performance of the In Situ ^{14}C Extraction Line at the University of Bern. *Radiocarbon* 62: 1371–88.

Sliz, M. U., Hofmann, B. A., Leya, I., Szidat, S., Espic, C., Gattacceca, J., Braucher, R., Borschineck, D., Gnos, E., and ASTER Team. 2022. Terrestrial Ages of Seven Meteorite Strewn Fields and Two Single Unpaired Meteorites from the Sultanate of Oman Determined Using ^{14}C and ^{10}Be. *Meteoritics & Planetary Science* 57: 2170–91.

Szidat, S. 2020. ^{14}C Research at the Laboratory of the Analysis of Radiocarbon with AMS (LARA), University of Bern. *CHIMIA* 74: 1010–14.

Szidat, S., Salazar, G. A., Vogel, E., Battaglia, M., Wacker, L., Synal, H. A., and Türler, A. 2014. ^{14}C Analysis and Sample Preparation at the New Bern Laboratory for the Analysis of Radiocarbon with AMS (LARA). *Radiocarbon* 56: 561–66.

Vogt, S. K., Aylmer, D., Herzog, G. F., Wieler, R., Signer, P., Pellas, P., Fiéni, C., et al. 1993. On the Bur Gheluai H5 Chondrite and Other Meteorites with Complex Exposure Histories. *Meteoritics* 28: 71–85.

Welten, K. C., Nishiizumi, K., Masarik, J., Caffee, M. W., Jull, A. J. T., Klandrud, S. E., and Wieler, R. 2001. Cosmic-Ray Exposure History of Two Frontier Mountain H-Chondrite Showers from Spallation and Neutron-Capture Products. *Meteoritics & Planetary Science* 36: 301–317.

Wieler, R., Graf, T., Signer, P., Vogt, S., Herzog, G. F., Tuniz, C., Fink, D., et al. 1996. Exposure History of the Torino Meteorite. *Meteoritics & Planetary Science* 31: 265–272.